Scripta Materialia 127 (2017) 132–135

Contents lists available at ScienceDirect

Scripta Materialia

journal homepage: www.elsevier.com/locate/scriptamat

Regular article

Grain orientations and grain boundaries in tungsten nonotendril fuzz grown under divertor-like conditions☆

Chad M. Parish [a,*], Kun Wang [a], Russel P. Doerner [b], Matthew J. Baldwin [b]

[a] Oak Ridge National Laboratory, Oak Ridge, TN, USA
[b] University of California – San Diego, La Jolla, CA, USA

ARTICLE INFO

Article history:
Received 2 September 2016
Received in revised form 13 September 2016
Accepted 14 September 2016
Available online xxxx

Keywords:
Transmission Kikuchi diffraction
Plasma simulation
Fusion energy
Fusion
Tungsten

ABSTRACT

We grew nanotendril "fuzz" on tungsten via plasma exposure and performed transmission Kikuchi diffraction (tKD) in scanning electron microscopy of isolated nanotendrils. 900 °C, 10^{23} He/m^{2}sec, 4×10^{26} He/m^2 exposure of tungsten produced a deep and fully developed nanotendril mat. tKD of isolated nanotendrils indicated that there was no preferred crystallographic direction oriented along the long axes of the tendrils, and the grain boundary character showed slightly preferential orientations. Tendril growth is sufficiently non-equilibrium to prevent any preference of growth direction to manifest measurably, and that new high-angle boundaries (with new grains and grain-growth axes) nucleate randomly along the tendrils during growth.

In a magnetic fusion energy (MFE) system, such as a tokamak, the plasma-facing materials (PFMs) will be bombarded by a combination of deuterium/tritium ions and helium ions, while at high temperature and subjected to severe neutron irradiation. Tungsten is the primary candidate for the ITER project tokamak's divertors, and is the current front-runner for solid-wall and solid-divertor concepts in future tokamak designs [1]. However, nanostructure growth – so-called nanofuzz or nanotendrils, often microns long and ≪100 nm in diameter – develops on tungsten surfaces during helium bombardment, and are not presently understood in detail [2–7]. This is one of the factors that may limit the applicability of tungsten (or indeed, many materials [8]) in the plasma-materials interaction environment.

The present understanding of nanostructure formation is primarily informed by molecular dynamics (MD) or other theory approaches [9–18], with relatively limited (although valuable) experimental information [5,6,8,19–21]. Still poorly defined is how fuzz transitions from the short incipient state of early growth – well-studied by MD – into the long and stably-growing state during later growth. Under the earliest growth conditions (perhaps 10^{24} He/m^2 and below), before the fuzz develops, the surface of the tungsten begins to facet, and the degree and type of faceting on each grain is strongly related to the surface normal of the individual grains [22]. By the time the fuzz has grown into a developed and surface-covering mat (perhaps 10^{26} He/m^2 and higher), the surface appears uniform and underlying grains are not discernable. This must imply that by the time the fuzz reaches a steadily-growing condition, the different underlying grain orientations do not affect the tendril growth. We hypothesize two possible mechanisms for this: (1) A given nanotendril growth axis – that is, a given crystallographic direction along the long axes of the tendrils – is strongly preferred, and the underlying grain orientations rotate near the substrate/tendril interface into this particular orientation. Based on loop-punching arguments and surface energy arguments, this privileged axis might be ⟨111⟩ if found. Contrariwise, (2), it is possible that no particular tendril long-axis crystallographic direction is preferred, and growth can proceed roughly equally regardless of the underlying grain orientation, with no selection needed.

To test these two hypotheses, we used transmission Kikuchi diffraction (tKD) [23–25] to interrogate a large number of individual nanotendrils to obtain a statistical view of the tendril axes and the intra-tendril grain boundary characters. We found no discernable preference for any given long-axis orientation, which we interpret to support hypothesis (2) above.

Experimentally, a specimen of mirror-polished polycrystalline tungsten was exposed to a He plasma in PISCES-A at the University of

☆ Notice: This manuscript has been authored by UT-Battelle, LLC under Contract No. DE-AC05-00OR22725 with the U.S. Department of Energy. The United States Government retains and the publisher, by accepting the article for publication, acknowledges that the United States Government retains a non-exclusive, paid-up, irrevocable, world-wide license to publish or reproduce the published form of this manuscript, or allow others to do so, for United States Government purposes. The Department of Energy will provide public access to these results of federally sponsored research in accordance with the DOE Public Access Plan (http://energy.gov/downloads/doe-public-access-plan).

* Corresponding author.
E-mail address: parishcm@ornl.gov (C.M. Parish).

http://dx.doi.org/10.1016/j.scriptamat.2016.09.018
1359-6462/

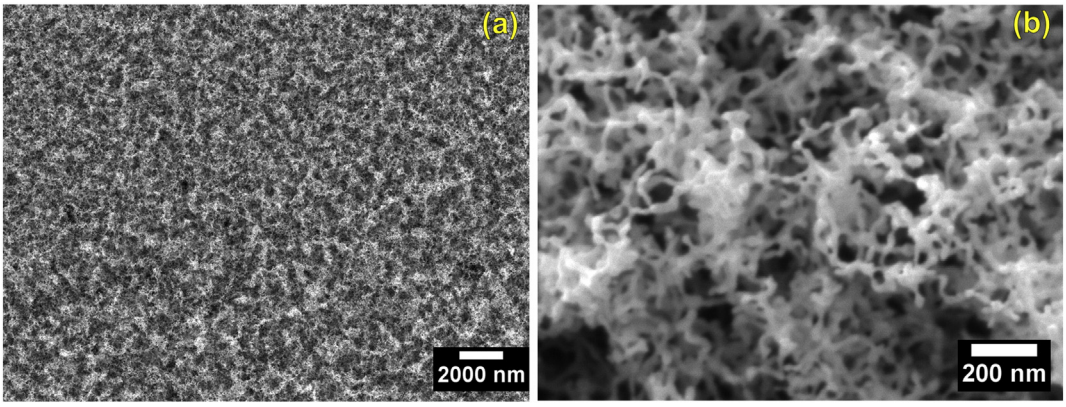

Fig. 1. Scanning electron micrographs of the surface of the nanotendril-coated tungsten surface.

California San Diego [26]. Conditions were 900 °C, 50 eV ion energy, ~10^{23} He/m^{2}s, 4000 s, to a total fluence of ~4×10^{26} He/m^2. The result is a thick (~1000 nm) mat of well-developed fuzz tendrils, of diameter ~20–30 nm; Fig. 1. It is also notable that the substrate grain size (roughly 1 μm) is much smaller than the field of view in Fig. 1a, but no grain contrast propagates to the surface, as noted above.

Samples for transmission Kikuchi diffraction were prepared by putting a drop of methanol onto the fuzzy surface, putting a drop of methanol onto a 3 mm ∅ copper-mesh TEM grid with a continuous carbon film covering it, gripping the copper grid with tweezers, and then swiping the grid across the surface of the fuzzy sample.

SEM imaging and tKD were performed with a JEOL JSM6500F field-emission scanning electron microscope (SEM). tKD was performed using an EDAX Hikari I electron backscatter diffraction (EBSD) system and OIM software suite v7. If the usual sense of sample tilt for EBSD is considered positive, the tKD samples were run with 30° tilt in the negative sense. Samples were mapped with 6–7 mm working distance, 25–30 keV accelerating potential, and 3–5 nA probe current. Scans were typically a few hundred nanometers on a side, with 5–10 nm pixel pitches, 2×2 or 4×4 pixel binning on the EBSD camera, and 10–20pixels/s. Scans were kept short (<5 min) to ensure negligible sample drift. Data cleaning consisted only of removing pixels of low image quality; no dilation, neighbor correlation, or other destructive cleanup steps were performed in post-processing [27]. A "mag-I-cal" specimen,[1] made from ⟨001⟩ orientated silicon with ⟨101⟩ in plane, and known spacings of SiGe layers, thinned by ion milling, was examined to confirm that tKD measured orientations to better than ±5° to the outside world, and magnifications to better than 20%. All of the patterns were saved during mapping, for later reindexing and reanalysis if necessary. The only phase identified was BCC tungsten, space group $Im\bar{3}m$.

Thirteen tendrils or tendril clusters were interrogated via tKD; Fig. 2a shows a typical SEM image. The image quality (IQ) map, which shows the sharpness of the tKD patterns on the EBSD camera and are therefore maps of the patterns' quality, are shown in Fig. 2b. A map of the crystallographic orientation in the out-of-the-page orientation, colored according to the inset unit triangle, is presented in Fig. 2c. Black lines denote high angle (>15°) grain boundaries, and cyan lines denote low angle (2–15°) boundaries. In Fig. 2b and c, two small marks, 'd' and 'e,' denote two typical tKD patterns that are presented as Figs. 2d-2e. Although the patterns are not excellent, mainly due to the necessity for dynamic background subtraction, they are fully suitable for consistent indexing if significant care is exercised in choosing the Hough transform parameters. Similar results are seen from another dataset, Fig. 3a–c.

The important point to take away from the data in Figs. 2–3, and the eleven other datasets we obtained similarly is that both intratendril grain boundaries are present, and the tendrils are generally only one grain wide, which means a given orientation down the tendril axis can be obtained for most grains.

Interestingly, and perhaps surprisingly, no preferred tendril growth axis is observed, Fig. 4a (and online Supplemental information Fig. S1). If there is a preferred axis, it is too statistically weak to be observed here. The unit triangle in Fig. 4a can hold all of the tendril long-axes orientations (due to tungsten's symmetry), and the points for individual grains ($N = 34$) are spread across the unit triangle. We also measured the axis/angle pairs that describe the grain boundaries, and plotted these in Figs. 4b–c. In Fig. 4b, the axis/angle pairs are plotted on the unit triangle at the axis location, and the points are sized and colored by the angle. The histogram of angles alone, Fig. 4c, shows a very slight preference at 60°, but generally a random assortment of angles. Note that for angles between 58 and 62°, the points are colored red to denote this narrow range of angles in a noticeable fashion. In the grain boundary analyses, no low-angle boundaries (<15°) were examined. For all of the data in Fig. 4, we used the "$\bar{g}$" option in EDAX OIM Analysis software, meaning that the average orientation of the grains, rather than the particular pixel within a grain selected by the computer mouse, was used to determine the tendril long axes or grain boundary axis/angle pairs.

We return to the two hypotheses stated in the introduction: (1) A given nanotendril growth axis is strongly preferred, leading to rotation of the tendril axes from the substrate into the preferred orientation, or (2) no particular tendril long-axis crystallographic direction is preferred, and growth can proceed roughly equally regardless of the underlying grain, with no selection needed. Our results, in which no preferential long axis is observed in a data with reasonable ($N = 34$) statistics, appear to support hypothesis (2). Because the tendrils are polycrystalline, with widely varying grain orientations within a single grain, we can in fact conclude that not only are given orientations not preferred, but the orientation of a single grain in a tendril need have no relationship to the underlying substrate grain.

The {101} plane has the lowest surface energy in tungsten, and the slip plane of punched prismatic loops – the presumed mechanism of at least early-stage tendril growth [11] – is {101}, with a slip direction of ⟨111⟩ [28]. Therefore, it might be expected that tendrils would have a ⟨111⟩ long axis, with {101} low-energy planes bounding the faces of the tendril with normals roughly perpendicular to the <111⟩ length. Clearly, from our tKD measurements, this is not occurring, but rather a uniform and random array of long axes are present.

It seems likely that at the high temperatures and high fluxes relevant to nanotendril growth, surface adatoms produced by loop-punching events may have time to undergo surface diffusion and lose their identity as punched loops, and attach to a convenient new location on the growing tendril. (What would make a particular location convenient, however, is not a question we can answer from

[1] http://www.technoorg.hu/product/magical/description/

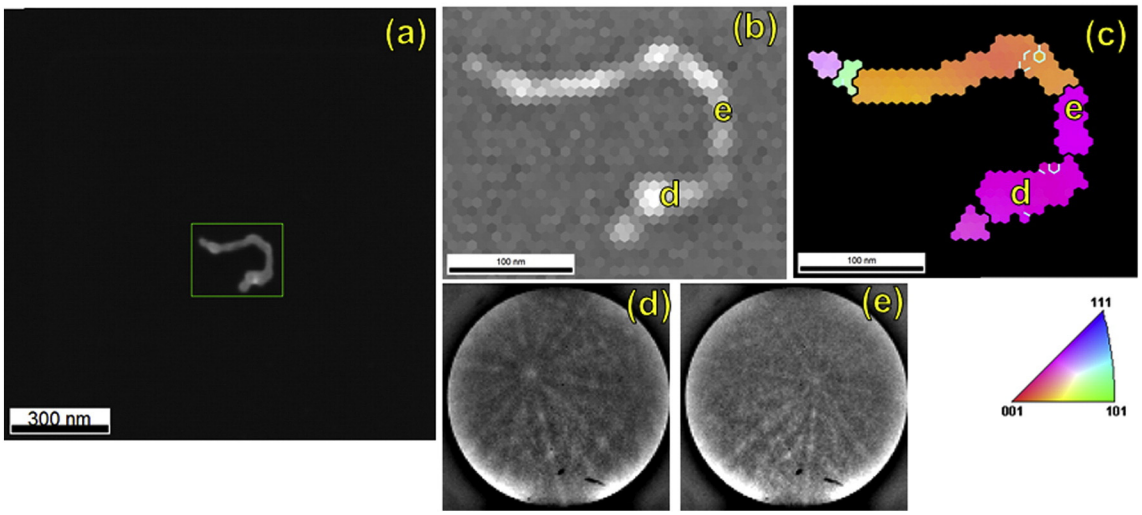

Fig. 2. (a) SEM image of an isolated tungsten nanotendril on a continuous carbon film. The green box denotes the area of tKD mapping. (b) Image quality map. (c) Z-axis (out-of-the-page) inverse pole figure colored map. Coloration is by the inset unit triangle. Black boundaries are high angle, cyan boundaries low-angle. (d–e) Typical tKD patterns from the marked points. Pixel pitch: 8 nm. (For interpretation of the references to color in this figure legend, the reader is referred to the web version of this article.)

this study.) The very high flux (~10^{23} He/m^2sec, or in a perspective more amenable to the size scale of these experiments, 100,000 He/nm^2sec) will produce a continuous perturbation of the evolving structure and probably make selection of a thermodynamically preferred orientation very difficult.

The grain boundaries' lack of preferred axes and nearly-random distribution of angles also implies lack of preferential selection; however, the grain boundary axis-angles pairs to not appear to be entirely random (see Supplemental information Figs. S2–S3). The preference towards the (111)-(101) zone and towards higher angles is more than can easily be attributed to random chance. Previously, work on deformed nanocrystalline tantalum [29] showed nanotwinning in this related BCC-structured metal, so it is worth future investigation if nanotwins are appearing regularly in plasma-damaged tungsten.

It is somewhat surprising that there is not a skew towards lower-angle grain boundaries. (We did not measure the LAGBs in Fig. 4, because so few were observed in these experiments.) If tendrils grew by a continuous extrusion of the underlying grain, we might expect a gradual rotation of the crystal lattice as the tendril twisted or turned, leading to occasional subgrain low-angle boundaries formed to relax the strain associated with the continuous buildup of strain. However, relatively few low angle boundaries were observed (i.e., Figs. 2–3), and most of the boundaries were high angle. This may imply an occasional nucleation of a new grain with a random orientation, rather than a continuous lattice rotation. This leads to questions that need to be addressed in future work, but the point that can be concluded here is that small rotations within grains are accommodated by occasional low-angle grain boundaries, but high-angle grain boundaries form every 30–100 nm, presumably to accommodate the growth strain. We will perform follow-up experiments comparing tKD to transmission electron microscopy (TEM) to determine if helium bubbles or other microstructural features are preferentially formed at these high-angle boundaries; a large bubble, for instance, would reduce the aggregate grain boundary area and lower the energetic penalty of forming a tungsten-tungsten high-angle boundary (but would have to balance against the energy of the bubble). In fig. 3c, for instance, the yellow-colored grain shows several unindexed (black) pixels in its center, where the low-angle grain boundaries meet. These dead pixels could conceivably be a bubble or bubble cluster, which is reducing the aggregate metal thickness in the beam direction and therefore leading to a reduced scattering intensity and concomitant inability to index the pixels' tKD patterns [30].

Oddly, multiple grain boundaries fall near the 60°{111} axis-angle pair. Although the 60°{111} boundary is the coherent twin Σ3 boundary in FCC structures, but in BCC structures it is a random boundary. The Σ3 boundaries are at 70.53°{112} or 109.47°{111} [31,32]. Thus, the slight preference to 60°{111} boundaries in this BCC structure is somewhat surprising, and difficult to explain. Manual indexing of stored EBSD patterns (e.g., Fig. 2d–e), however, confirms that these boundaries are correctly indexed.

In summary, we have used transmission Kikuchi diffraction to examine the grain structures of isolated tungsten nanotendrils grown under divertor-like plasma conditions. No preferred crystallographic direction was found in the grains' long axes along the tendrils' growth directions, which likely implies that growth is sufficiently fast and non-equilibrium

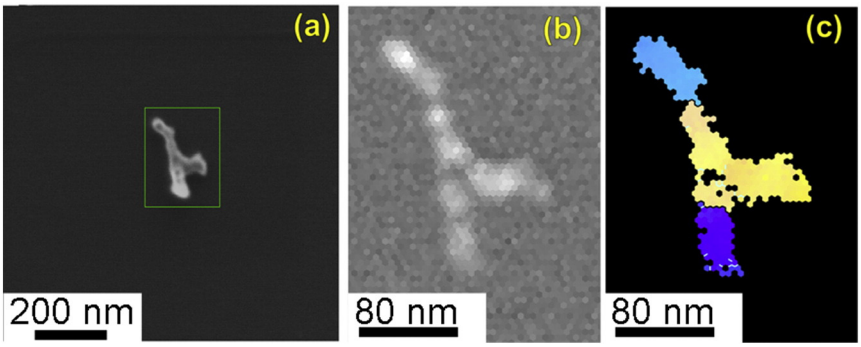

Fig. 3. (a) SEM, (b) image quality, and (c) Z-axis IPF maps from another tendril. In (c), colors and boundaries are the same as Fig. 2c. Pixel pitch: 5 nm.

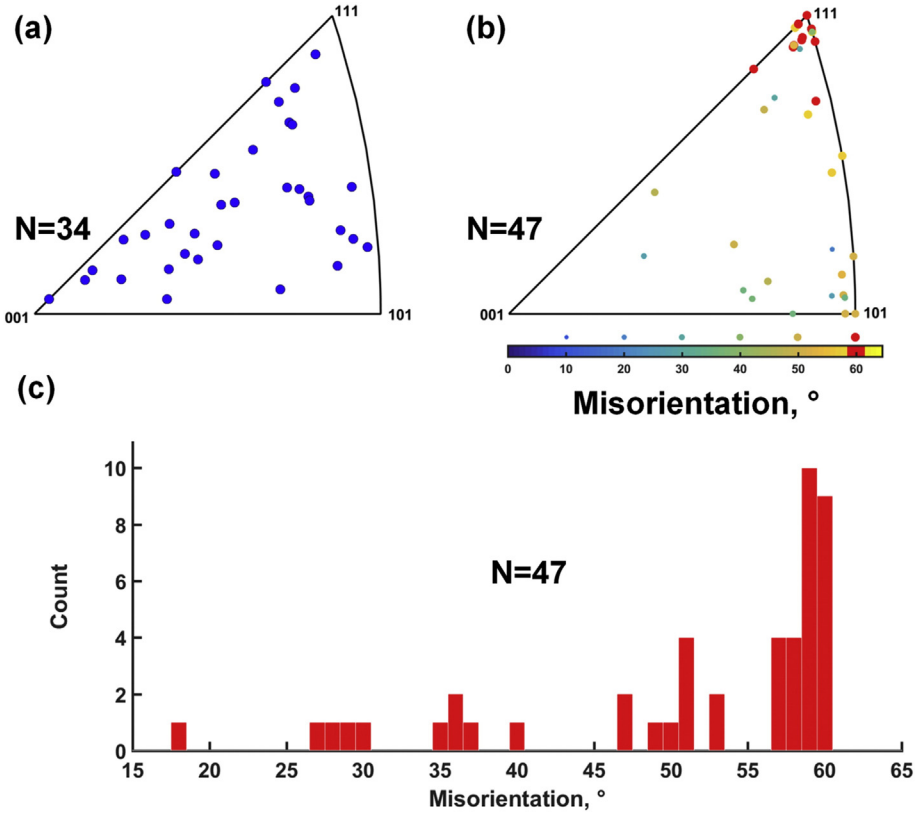

Fig. 4. (a) Long axes of the tendril grains. (b) Axis/angle pairs of the tendril grain boundaries. (c) Histogram of the grain boundary misorientation axes. No grain boundaries < 15° analyzed.

that any preferences from thermodynamics or dislocation slip for a given axis is overwhelmed by the rapid growth, allowing random growth orientations. There is a slight preference for certain high-angle axis/angle pairs in the grain boundary distribution, but an explanation will require further investigations.

Acknowledgements

CMP and KW supported by an Early Career Award, US Department of Energy, Office of Science, Fusion Energy Sciences under contract number DE-AC05-00OR22725. RPD and MJB supported by DE-FG02-07ER54912. We thank Prof B. Wirth, Dr. X. Hu., and Dr. D. Leonard for constructive criticism and discussions.

Appendix A. Supplementary data

Supplementary data to this article can be found online at http://dx.doi.org/10.1016/j.scriptamat.2016.09.018.

References

[1] T.J. Dolan, R.W. Moir, W. Manheimer, L.C. Cadwallader, M.J. Neumann, Magnetic Fusion Technology, Springer, 2013.
[2] M.J. Baldwin, R.P. Doerner, Nucl. Fusion 48 (2008) 035001.
[3] M.J. Baldwin, T.C. Lynch, R.P. Doerner, J.H. Yu, J. Nucl. Mater. 415 (2011) S104–S107.
[4] M.J. Baldwin, R.P. Doerner, J. Nucl. Mater. 404 (2010) 165–173.
[5] G.M. Wright, D. Brunner, M.J. Baldwin, R.P. Doerner, B. Labombard, B. Lipschultz, J.L. Terry, D.G. Whyte, Nucl. Fusion 52 (2012).
[6] G.M. Wright, D. Brunner, M.J. Baldwin, K. Bystrov, R.P. Doerner, B. Labombard, B. Lipschultz, G. De Temmerman, J.L. Terry, D.G. Whyte, K.B. Woller, J. Nucl. Mater. 438 (2013) S84–S89.
[7] S. Kajita, W. Sakaguchi, N. Ohno, N. Yoshida, T. Saeki, Nucl. Fusion 49 (2009).
[8] S. Takamura, Y. Uesugi, Appl. Surf. Sci. 356 (2015) 888–897.
[9] L. Hu, K.D. Hammond, B.D. Wirth, D. Maroudas, J. Appl. Phys. 118 (2015) 163301.
[10] L. Hu, K.D. Hammond, B.D. Wirth, D. Maroudas, J. Appl. Phys. 115 (2014) 173512.
[11] F. Sefta, K.D. Hammond, N. Juslin, B.D. Wirth, Nucl. Fusion 53 (2013) 073015.
[12] A. Ito, A. Takayama, Y. Oda, T. Tamura, R. Kobayashi, T. Hattori, S. Ogata, N. Ohno, S. Kajita, M. Yajima, Nucl. Fusion 55 (2015) 073013.
[13] L. Pentecoste, P. Brault, A.-L. Thomann, P. Desgardin, T. Lecas, T. Belhabib, M.-F. Barthe, T. Sauvage, J. Nucl. Mater. 470 (2016) 44–54.
[14] T. Faney, B.D. Wirth, Model. Simul. Mater. Sci. Eng. 22 (2014).
[15] A. Lasa, S. Tähtinen, K. Nordlund, EPL (Europhysics Letters) 105 (2014) 25002.
[16] S. Krasheninnikov, R. Smirnov, Nucl. Fusion 55 (2015) 073005.
[17] R. Smirnov, S. Krasheninnikov, J. Guterl, J. Nucl. Mater. 463 (2015) 359–362.
[18] J. Wang, L.-L. Niu, X. Shu, Y. Zhang, J. Phys. Condens. Matter 27 (2015) 395001.
[19] O. El-Atwani, G. Sean, E. Mert, T. Gregory De, M. Thomas, B. Kirill, K. Daniel, Q. Tian, J.P. Allain, Nucl. Fusion 54 (2014) 083013.
[20] P. Fiflis, D. Curreli, D. Ruzic, Nucl. Fusion 55 (2015) 033020.
[21] M. Efe, O. El-Atwani, Y. Guo, D.R. Klenosky, Scr. Mater. 70 (2014) 31–34.
[22] C.M. Parish, H. Hijazi, H.M. Meyer III, F.W. Meyer, Acta Mater. 62 (2014) 173–181.
[23] P.W. Trimby, Ultramicroscopy 120 (2012) 16–24.
[24] R.R. Keller, R.H. Geiss, J. Microsc. 245 (2012) 245–251.
[25] S. Suzuki, JOM 65 (2013) 1254–1263.
[26] D. Goebel, G. Campbell, R. Conn, J. Nucl. Mater. 121 (1984) 277–282.
[27] L.N. Brewer, J.R. Michael, Microscopy Today 18 (2010) 10–15.
[28] N. Ohno, Y. Hirahata, M. Yamagiwa, S. Kajita, M. Takagi, N. Yoshida, R. Yoshihara, T. Tokunaga, M. Tokitani, Supplement 438 (2013) S879–S882.
[29] Y. Wang, A. Hodge, J. Biener, A. Hamza, D. Barnes, K. Liu, T. Nieh, Appl. Phys. Lett. 86 (2005) 101915.
[30] R. van Bremen, D.R. Gomes, L. de Jeer, V. Ocelík, J.T.M. De Hosson, Ultramicroscopy 160 (2016) 256–264.
[31] P. Lejcek, Grain Boundary Segregation in Metals, Springer Science & Business Media, 2010.
[32] N. Gao, C.-C. Fu, M. Samaras, R. Schäublin, M. Victoria, W. Hoffelner, J. Nucl. Mater. 385 (2009) 262–267.